Search for the standard model Higgs boson in e^+e^- collisions at $\sqrt{s}$=161, 170 and 172 GeV

R. Barate, D. Buskulic, D. Decamp, P. Ghez, C. Goy, J P. Lees, A. Lucotte, M N. Minard, J Y. Nief, B. Pietrzyk, et al.

CERN-PPE/97-70
June 17, 1997

Search for the Standard Model Higgs Boson in e^+e^- Collisions at $\sqrt{s} = 161$, 170 and 172 GeV

The ALEPH Collaboration*

Abstract

The reaction $e^+e^- \to HZ$ is used to search for the Standard Model Higgs boson. The data sample consists of integrated luminosities of $10.9\,pb^{-1}$, $1.1\,pb^{-1}$, and $9.5\,pb^{-1}$ collected by the ALEPH experiment at LEP during 1996, at centre-of-mass energies of 161, 170 and 172 GeV, respectively. No candidate events were found, in agreement with the expected background of 0.84 events from all Standard Model processes. This search results in a 95% C.L. lower limit on the Higgs boson mass of $69.4\,GeV/c^2$. When combined with earlier ALEPH searches performed at energies at and around the Z peak, this limit increases to $70.7\,GeV/c^2$.

Submitted to Physics Letters B

* See following pages for the list of authors

The ALEPH Collaboration

R. Barate, D. Buskulic, D. Decamp, P. Ghez, C. Goy, J.-P. Lees, A. Lucotte, M.-N. Minard, J.-Y. Nief, B. Pietrzyk

Laboratoire de Physique des Particules (LAPP), IN^{2}P^3-CNRS, 74019 Annecy-le-Vieux Cedex, France

M.P. Casado, M. Chmeissani, P. Comas, J.M. Crespo, M. Delfino, E. Fernandez, M. Fernandez-Bosman, Ll. Garrido,[15] A. Juste, M. Martinez, G. Merino, R. Miquel, Ll.M. Mir, C. Padilla, I.C. Park, A. Pascual, J.A. Perlas, I. Riu, F. Sanchez, F. Teubert

Institut de Física d'Altes Energies, Universitat Autònoma de Barcelona, 08193 Bellaterra (Barcelona), Spain[7]

A. Colaleo, D. Creanza, M. de Palma, G. Gelao, G. Iaselli, G. Maggi, M. Maggi, N. Marinelli, S. Nuzzo, A. Ranieri, G. Raso, F. Ruggieri, G. Selvaggi, L. Silvestris, P. Tempesta, A. Tricomi,[3] G. Zito

Dipartimento di Fisica, INFN Sezione di Bari, 70126 Bari, Italy

X. Huang, J. Lin, Q. Ouyang, T. Wang, Y. Xie, R. Xu, S. Xue, J. Zhang, L. Zhang, W. Zhao

Institute of High-Energy Physics, Academia Sinica, Beijing, The People's Republic of China[8]

D. Abbaneo, R. Alemany, A.O. Bazarko,[1] U. Becker, P. Bright-Thomas, M. Cattaneo, F. Cerutti, G. Dissertori, H. Drevermann, R.W. Forty, M. Frank, R. Hagelberg, J.B. Hansen, J. Harvey, P. Janot, B. Jost, E. Kneringer, J. Knobloch, I. Lehraus, G. Lutters, P. Mato, A. Minten, L. Moneta, A. Pacheco, J.-F. Pusztaszeri,[20] F. Ranjard, G. Rizzo, L. Rolandi, D. Rousseau, D. Schlatter, M. Schmitt, O. Schneider, W. Tejessy, I.R. Tomalin, H. Wachsmuth, A. Wagner[21]

European Laboratory for Particle Physics (CERN), 1211 Geneva 23, Switzerland

Z. Ajaltouni, A. Barrès, C. Boyer, A. Falvard, C. Ferdi, P. Gay, C . Guicheney, P. Henrard, J. Jousset, B. Michel, S. Monteil, J-C. Montret, D. Pallin, P. Perret, F. Podlyski, J. Proriol, P. Rosnet, J.-M. Rossignol

Laboratoire de Physique Corpusculaire, Université Blaise Pascal, IN^{2}P^3-CNRS, Clermont-Ferrand, 63177 Aubière, France

T. Fearnley, J.D. Hansen, J.R. Hansen, P.H. Hansen, B.S. Nilsson, B. Rensch, A. Wäänänen

Niels Bohr Institute, 2100 Copenhagen, Denmark[9]

G. Daskalakis, A. Kyriakis, C. Markou, E. Simopoulou, A. Vayaki

Nuclear Research Center Demokritos (NRCD), Athens, Greece

A. Blondel, J.C. Brient, F. Machefert, A. Rougé, M. Rumpf, A. Valassi,[6] H. Videau

Laboratoire de Physique Nucléaire et des Hautes Energies, Ecole Polytechnique, IN^{2}P^3-CNRS, 91128 Palaiseau Cedex, France

E. Focardi, G. Parrini, K. Zachariadou

Dipartimento di Fisica, Università di Firenze, INFN Sezione di Firenze, 50125 Firenze, Italy

R. Cavanaugh, M. Corden, C. Georgiopoulos, T. Huehn, D.E. Jaffe

Supercomputer Computations Research Institute, Florida State University, Tallahassee, FL 32306-4052, USA [13,14]

A. Antonelli, G. Bencivenni, G. Bologna,[4] F. Bossi, P. Campana, G. Capon, D. Casper, V. Chiarella, G. Felici, P. Laurelli, G. Mannocchi,[5] F. Murtas, G.P. Murtas, L. Passalacqua, M. Pepe-Altarelli

Laboratori Nazionali dell'INFN (LNF-INFN), 00044 Frascati, Italy

L. Curtis, S.J. Dorris, A.W. Halley, I.G. Knowles, J.G. Lynch, V. O'Shea, C. Raine, J.M. Scarr, K. Smith, P. Teixeira-Dias, A.S. Thompson, E. Thomson, F. Thomson, R.M. Turnbull

Department of Physics and Astronomy, University of Glasgow, Glasgow G12 8QQ,United Kingdom[10]

O. Buchmüller, S. Dhamotharan, C. Geweniger, G. Graefe, P. Hanke, G. Hansper, V. Hepp, E.E. Kluge, A. Putzer, J. Sommer, K. Tittel, S. Werner, M. Wunsch

Institut für Hochenergiephysik, Universität Heidelberg, 69120 Heidelberg, Fed. Rep. of Germany[16]

R. Beuselinck, D.M. Binnie, W. Cameron, P.J. Dornan, M. Girone, S. Goodsir, E.B. Martin, P. Morawitz, A. Moutoussi, J. Nash, J.K. Sedgbeer, P. Spagnolo, A.M. Stacey, M.D. Williams

Department of Physics, Imperial College, London SW7 2BZ, United Kingdom[10]

V.M. Ghete, P. Girtler, D. Kuhn, G. Rudolph

Institut für Experimentalphysik, Universität Innsbruck, 6020 Innsbruck, Austria[18]

A.P. Betteridge, C.K. Bowdery, P. Colrain, G. Crawford, A.J. Finch, F. Foster, G. Hughes, R.W. Jones, T. Sloan, E.P. Whelan, M.I. Williams

Department of Physics, University of Lancaster, Lancaster LA1 4YB, United Kingdom[10]

C. Hoffmann, K. Jakobs, K. Kleinknecht, G. Quast, B. Renk, E. Rohne, H.-G. Sander, P. van Gemmeren, C. Zeitnitz

Institut für Physik, Universität Mainz, 55099 Mainz, Fed. Rep. of Germany[16]

J.J. Aubert, C. Benchouk, A. Bonissent, G. Bujosa, J. Carr, P. Coyle, C. Diaconu, A. Ealet, D. Fouchez, N. Konstantinidis, O. Leroy, F. Motsch, P. Payre, M. Talby, A. Sadouki, M. Thulasidas, A. Tilquin, K. Trabelsi

Centre de Physique des Particules, Faculté des Sciences de Luminy, IN^{2}P^3-CNRS, 13288 Marseille, France

M. Aleppo, M. Antonelli, F. Ragusa[12]

Dipartimento di Fisica, Università di Milano e INFN Sezione di Milano, 20133 Milano, Italy.

R. Berlich, W. Blum, V. Büscher, H. Dietl, G. Ganis, C. Gotzhein, H. Kroha, G. Lütjens, G. Lutz, W. Männer, H.-G. Moser, R. Richter, A. Rosado-Schlosser, S. Schael, R. Settles, H. Seywerd, R. St. Denis, H. Stenzel, W. Wiedenmann, G. Wolf

Max-Planck-Institut für Physik, Werner-Heisenberg-Institut, 80805 München, Fed. Rep. of Germany[16]

J. Boucrot, O. Callot,[12] S. Chen, A. Cordier, M. Davier, L. Duflot, J.-F. Grivaz, Ph. Heusse, A. Höcker, A. Jacholkowska, M. Jacquet, M. Kado, D.W. Kim,[2] F. Le Diberder, J. Lefrançois, A.-M. Lutz, I. Nikolic, M.-H. Schune, L. Serin, S. Simion, E. Tournefier, J.-J. Veillet, I. Videau, D. Zerwas

Laboratoire de l'Accélérateur Linéaire, Université de Paris-Sud, IN^{2}P^3-CNRS, 91405 Orsay Cedex, France

P. Azzurri, G. Bagliesi, S. Bettarini, C. Bozzi, G. Calderini, V. Ciulli, R. Dell'Orso, R. Fantechi, I. Ferrante, A. Giassi, A. Gregorio, F. Ligabue, A. Lusiani, P.S. Marrocchesi, A. Messineo, F. Palla, G. Sanguinetti, A. Sciabà, J. Steinberger, R. Tenchini, C. Vannini, A. Venturi, P.G. Verdini

Dipartimento di Fisica dell'Università, INFN Sezione di Pisa, e Scuola Normale Superiore, 56010 Pisa, Italy

G.A. Blair, L.M. Bryant, J.T. Chambers, Y. Gao, M.G. Green, T. Medcalf, P. Perrodo, J.A. Strong, J.H. von Wimmersperg-Toeller

Department of Physics, Royal Holloway & Bedford New College, University of London, Surrey TW20 OEX, United Kingdom[10]

D.R. Botterill, R.W. Clifft, T.R. Edgecock, S. Haywood, P. Maley, P.R. Norton, J.C. Thompson, A.E. Wright

Particle Physics Dept., Rutherford Appleton Laboratory, Chilton, Didcot, Oxon OX11 OQX, United Kingdom[10]

B. Bloch-Devaux, P. Colas, B. Fabbro, W. Kozanecki, E. Lançon, M.C. Lemaire, E. Locci, P. Perez, J. Rander, J.-F. Renardy, A. Rosowsky, A. Roussarie, J.-P. Schuller, J. Schwindling, A. Trabelsi, B. Vallage

CEA, DAPNIA/Service de Physique des Particules, CE-Saclay, 91191 Gif-sur-Yvette Cedex, France[17]

S.N. Black, J.H. Dann, H.Y. Kim, A.M. Litke, M.A. McNeil, G. Taylor

Institute for Particle Physics, University of California at Santa Cruz, Santa Cruz, CA 95064, USA[19]

Department of Physics, University of Sheffield, Sheffield S3 7RH, United Kingdom[10]

K. Affholderbach, A. Böhrer, S. Brandt, G. Cowan, J. Foss, C. Grupen, P. Saraiva, L. Smolik, F. Stephan

Fachbereich Physik, Universität Siegen, 57068 Siegen, Fed. Rep. of Germany[16]

M. Apollonio, L. Bosisio, R. Della Marina, G. Giannini, B. Gobbo, G. Musolino

Dipartimento di Fisica, Università di Trieste e INFN Sezione di Trieste, 34127 Trieste, Italy

J. Putz, J. Rothberg, S. Wasserbaech, R.W. Williams

Experimental Elementary Particle Physics, University of Washington, WA 98195 Seattle, U.S.A.

S.R. Armstrong, E. Charles, P. Elmer, D.P.S. Ferguson, S. González, T.C. Greening, O.J. Hayes, H. Hu, S. Jin, P.A. McNamara III, J.M. Nachtman, J. Nielsen, W. Orejudos, Y.B. Pan, Y. Saadi, I.J. Scott, J. Walsh, Sau Lan Wu, X. Wu, J.M. Yamartino, G. Zobernig

Department of Physics, University of Wisconsin, Madison, WI 53706, USA[11]

[1]Now at Princeton University, Princeton, NJ 08544, U.S.A.

[2]Permanent address: Kangnung National University, Kangnung, Korea.

[3]Also at Dipartimento di Fisica, INFN Sezione di Catania, Catania, Italy.

[4]Also Istituto di Fisica Generale, Università di Torino, Torino, Italy.

[5]Also Istituto di Cosmo-Geofisica del C.N.R., Torino, Italy.

[6]Supported by the Commission of the European Communities, contract ERBCHBICT941234.

[7]Supported by CICYT, Spain.

[8]Supported by the National Science Foundation of China.

[9]Supported by the Danish Natural Science Research Council.

[10]Supported by the UK Particle Physics and Astronomy Research Council.

[11]Supported by the US Department of Energy, grant DE-FG0295-ER40896.

[12]Also at CERN, 1211 Geneva 23,Switzerland.

[13]Supported by the US Department of Energy, contract DE-FG05-92ER40742.

[14]Supported by the US Department of Energy, contract DE-FC05-85ER250000.

[15]Permanent address: Universitat de Barcelona, 08208 Barcelona, Spain.

[16]Supported by the Bundesministerium für Bildung, Wissenschaft, Forschung und Technologie, Fed. Rep. of Germany.

[17]Supported by the Direction des Sciences de la Matière, C.E.A.

[18]Supported by Fonds zur Förderung der wissenschaftlichen Forschung, Austria.

[19]Supported by the US Department of Energy, grant DE-FG03-92ER40689.

[20]Now at School of Operations Research and Industrial Engireering, Cornell University, Ithaca, NY 14853-3801, U.S.A.

[21]Now at Schweizerischer Bankverein, Basel, Switzerland.

1 Introduction

In the minimal Standard Model, the spontaneous breaking of $\mathrm{SU}(2)_L \times \mathrm{U}(1)_Y$ is achieved at the expense of the introduction of a doublet of complex scalar fields ϕ in self-interaction. As ϕ develops a vacuum expectation value, the W and Z bosons acquire their masses while three of the four initial degrees of freedom are absorbed. A single neutral scalar particle remains, the Higgs boson H. The mass of the Higgs boson is not specified by the theory, but for a given mass the theory predicts its production rates and partial decay widths unambiguously [1].

At LEP 1, the Higgs-strahlung process $\mathrm{e^+e^-} \to \mathrm{HZ^*} \to \mathrm{Hf\bar{f}}$ (Fig. 1a) was the dominant Higgs boson production mechanism. This process was investigated by ALEPH [2] in the $\mathrm{H}\nu\bar{\nu}$ and $\mathrm{H}\ell^+\ell^-$ channels (throughout this paper ℓ denotes an electron or a muon) with the whole data sample collected at centre-of-mass energies in the vicinity of the Z peak. This sample corresponds to over 4.5 million hadronic Z decays. Three events were observed, in agreement with the expected background, and a 95% C.L. lower limit on the Standard Model Higgs boson mass was set at $63.9\,\mathrm{GeV}/c^2$. Excluded domains up to $60.2\,\mathrm{GeV}/c^2$ were also reported by the other LEP experiments [3]. The LEP 1 analyses, however, were slowly reaching their limit in terms of search sensitivity, because the production cross section rapidly vanishes with increasing m_{H} (see Fig. 1b).

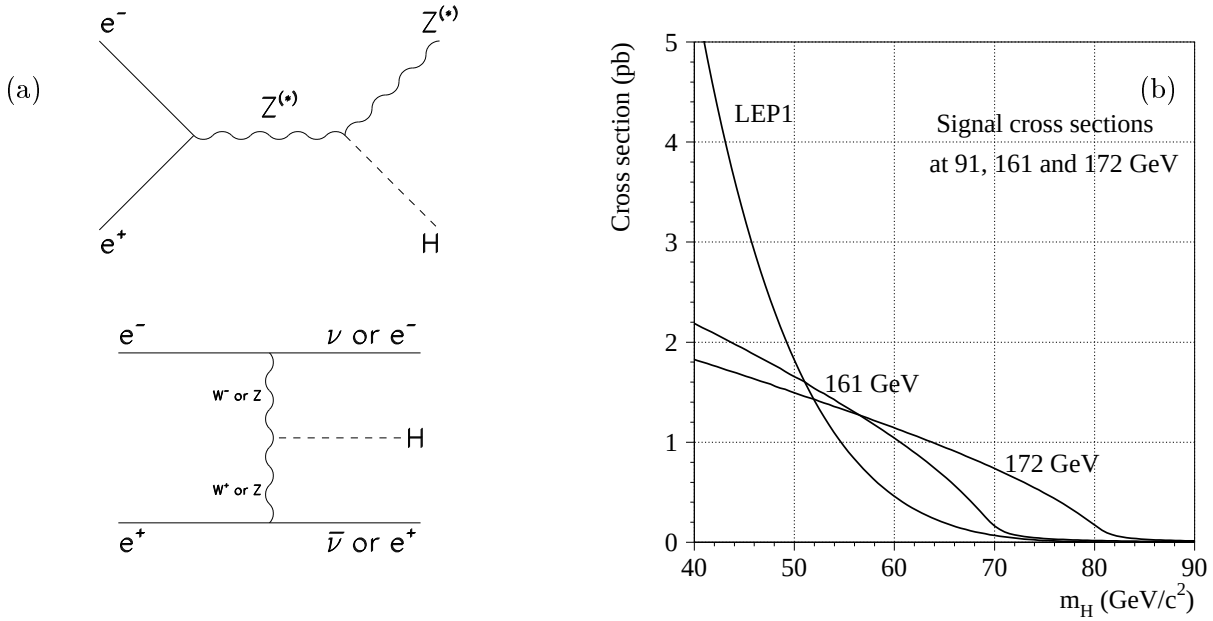

Figure 1: (a) Feynman diagrams for the Higgs-strahlung process (top) and for the WW or ZZ fusion process (bottom); and (b) corresponding production cross sections as a function of the Higgs boson mass at LEP 1 energies, at 161 GeV and at 172 GeV.

During 1996, the LEP centre-of-mass energy was increased to 161 GeV, and subsequently to 172 GeV. Due to the possibility of producing an on-shell Z boson in association with a Higgs boson, still via the Higgs-strahlung process $\mathrm{e^+e^-} \to \mathrm{HZ}$, the production cross section is sizeable for Higgs boson masses up to $m_{\mathrm{H}} \simeq \sqrt{s} - m_{\mathrm{Z}}$. The production cross sections at the Z peak and at the higher energies are displayed in Fig. 1b as a function of the Higgs boson mass, including

a small contribution from WW and ZZ fusion (Fig. 1a). A sensitivity to $m_{\mathrm{H}} \sim 60$ GeV/c^2 has already been achieved by OPAL [4] with an integrated luminosity of $10\,\mathrm{pb}^{-1}$ collected at 161 GeV.

With the integrated luminosity recorded by ALEPH at 161.3 GeV ($10.9\,\mathrm{pb}^{-1}$), 170.3 GeV ($1.1\,\mathrm{pb}^{-1}$) and 172.3 GeV ($9.5\,\mathrm{pb}^{-1}$), about ten events are expected to be produced if $m_{\mathrm{H}} = 70\,\mathrm{GeV}/c^2$. To be able to select a significant fraction of these ten events, all the final states are considered. These final states depend on the decay modes of the Z ($\ell^+\ell^-$, $\tau^+\tau^-$, $\nu\bar{\nu}$ and $\mathrm{q\bar{q}}$) and the Higgs boson ($\mathrm{b\bar{b}}$, $\tau^+\tau^-$, $\mathrm{c\overline{c}}$ and gg). These final states are addressed by five selections, namely $\mathrm{H}\ell^+\ell^-$, $\mathrm{H}\nu\bar{\nu}$, $\mathrm{Hq\bar{q}}$, $\mathrm{H}\tau^+\tau^-$ and $\tau^+\tau^-\mathrm{q\bar{q}}$. The $\tau^+\tau^-\mathrm{q\bar{q}}$ analysis supplements the $\mathrm{Hq\bar{q}}$ selection in cases where the Higgs boson decays to $\tau^+\tau^-$. The $\mathrm{H}\tau^+\tau^-$ and $\tau^+\tau^-\mathrm{q\bar{q}}$ selections are treated together due to the similar topology.

Several differences between the situation at LEP 2 and at the Z peak can be pointed out. Due to the larger number of channels, the statistical treatment of analysis optimization and combination is more involved. Also, at LEP 1 the background to the Higgs boson search in the $\mathrm{H}\nu\bar{\nu}$ channel consists mainly of $\mathrm{e^+e^-} \to \mathrm{q\bar{q}}$ events with extreme energy losses due to detector effects or exotic heavy quark semileptonic decays. Since the production cross section of these processes is several orders of magnitude smaller at LEP 2 than at the Z peak, background of this type is no longer significant. Instead, the background is due mainly to calculable physics processes. Consequently, the prediction of the background no longer depends upon details of the detector simulation or the knowledge of rare physical processes. It is therefore more reliable at LEP 2 than at LEP 1, and the analysis can be designed to exploit this good theoretical knowledge. A similar situation holds in the other decay channels as well. The lower cross sections for the background processes also allow Monte Carlo samples to be produced with an equivalent luminosity much larger than the actual recorded luminosity.

Finally, the Z boson produced in association with the Higgs boson via the Higgs-strahlung process is produced on-shell at LEP 2 energies, while it was highly virtual at LEP 1. This additional mass constraint allows the Higgs boson mass to be reconstructed with a good resolution in all channels, thus enhancing the discriminating power of all analyses with respect to simple event counting.

This letter is organized as follows. After a brief description of the ALEPH detector in Section 2, the important issues relevant for the search strategy, the selection optimization and the analysis combination, are addressed in Section 3. In Section 4, the background studies and the searches for the various final states are presented in detail. The combination and the final results are described in Section 5.

2 The ALEPH Detector

A detailed description of the ALEPH detector and its performance can be found in Refs. [5] and [6]. The only major modification to the apparatus took place in October 1995 when the vertex detector was replaced by a new device [7], twice as long as the previous one. The new device extends the acceptance to lower polar angles and has less material in the active region. Charged particle tracking is achieved with the new vertex detector, a cylindrical drift chamber and a

large time projection chamber. A 1.5 T axial magnetic field is provided by a superconducting solenoidal coil. A $1/p_{\rm t}$ resolution of 6×10^{-4} (GeV/c)$^{-1}\oplus5\times10^{-3}/p_{\rm t}$ is achieved, and the three-dimensional impact parameter resolution can be parametrized as $(34{+}70/p){\times}(1{+}1.6\cos^4\theta)$ μm, with p in GeV/c. Hereafter, charged particle tracks reconstructed with at least four hits in the time projection chamber and originating from within a cylinder of length 20 cm and radius 2 cm coaxial with the beam and centred at the nominal collision point are called *good tracks*. Throughout this letter, events with at least five good tracks accounting for more than 10% of the centre-of-mass energy are referred to as *hadronic events*.

Electrons and photons are identified in the electromagnetic calorimeter by their characteristic longitudinal and transverse shower developments [6]. The calorimeter, a lead/wire-plane sampling device with fine readout segmentation and total thickness of 22 radiation lengths at normal incidence, provides a relative energy resolution of $0.18/\sqrt{E}+0.009$ (E in GeV).

Muons are identified by their characteristic penetration pattern in the hadron calorimeter [6], a 1.2 m thick yoke instrumented with 23 layers of streamer tubes, together with two surrounding layers of muon chambers. In association with the electromagnetic calorimeter, the hadron calorimeter also provides a measurement of the energy of charged and neutral hadrons with a relative resolution of $0.85/\sqrt{E}$ (E in GeV).

The total visible energy, and therefore also the missing energy, is measured with an energy-flow reconstruction algorithm [6] which combines all of the above measurements, supplemented by the energy detected at low polar angles by two additional electromagnetic calorimeters which are used principally for the luminosity determination. In addition to the total energy measurement, the energy-flow reconstruction algorithm also provides a list of charged and neutral reconstructed objects, called *energy-flow particles*, allowing jets to be reconstructed with a typical angular resolution of 20 mrad both for the polar and azimuthal angles, and a relatively uniform energy resolution over the whole detector acceptance. The latter can be parametrized as $\sigma_E=(0.60\sqrt{E}+0.6)\,\mathrm{GeV}\times(1+\cos^2\theta)$ where E (in GeV) and θ are the jet energy and polar angle, respectively.

Finally, jets originating from b quarks are identified from lifetime b tagging algorithms [8], from high transverse momentum leptons coming from semileptonic decays [9], and from jet shape variables such as charged multiplicity, boosted sphericity, and sum of the transverse momenta squared with respect to the jet axes. These quantities are combined with a neural network into a single variable η_i for each jet i, where η_i is near unity for tagged b jets and near zero for other jets. The neural network b tagging is described in detail in Ref. [10].

In the data sample used for the analysis reported here, all major components of the detector were required to be simultaneously operational, and all major trigger logic had to be enabled.

3 Search Strategy

3.1 Monte Carlo Samples

To design the selection algorithms, large Monte Carlo samples were generated for all background and signal processes, and processed through the complete detector simulation and event reconstruction. To fully benefit from the good theoretical knowledge of the background, a luminosity equivalent in most cases to about 100 times the luminosity recorded in ALEPH was simulated for each process. The samples available at 172 GeV are summarized in Table 1.

Table 1: Number of events generated (in thousands) for each background process, and the equivalent luminosity (with the corresponding scaling factor with respect to the actual data sample), at a centre-of-mass energy of 172 GeV. A private generator was used for the process $e^+e^- \to Z\nu\bar{\nu}$ [11]. All other processes were generated with PYTHIA [12]. In this table, Z is used to represent Z or γ^*. Cuts of $0.2\,\mathrm{GeV}/c^2$ and $12\,\mathrm{GeV}/c^2$ are placed on the Z mass for the ZZ and Ze^+e^- final states, respectively. The mass of the hadronic system was required to be larger than $30\,\mathrm{GeV}/c^2$ for the process $\gamma\gamma \to q\bar{q}$.

Process	No. Events (10^3)	$\mathcal{L}$ (fb^{-1})
$e^+e^- \to q\bar{q}$	325	2.68 (253)
$e^+e^- \to W^+W^-$	12	1.02 (96)
$e^+e^- \to ZZ$	3	0.98 (92)
$e^+e^- \to We\nu$	1	2.07 (195)
$e^+e^- \to Ze^+e^-$	7	1.07 (101)
$e^+e^- \to Z\nu\bar{\nu}$	0.1	10.0 (943)
$\gamma\gamma \to q\bar{q}$	200	0.25 (24)

Signal events were generated with the HZHA program [13]. At least 2,000 events were simulated for each of the various final states, for Higgs boson masses varying from 45 to $80\,\mathrm{GeV}/c^2$, and at each centre-of-mass energy.

3.2 Selection Optimization

The above Monte Carlo samples are first used to identify variables discriminating signal and background events. These quantities are described in detail in the following sections, for each of the final states. As had already been the case for LEP 1 analyses [2], the locations of the cuts on the most critical variables are placed in such a way that, if the Higgs boson is too heavy to be produced at LEP (the null hypothesis), the highest 95% C.L. lower limit on its mass is achieved, on average.

To do so, an estimator, inspired by Ref. [14], is built to rank all possible experiment outcomes from the least to the most signal-like, using both the number of selected events and their distribution of reconstructed Higgs boson candidate masses [15]. For any experiment outcome, a confidence level $c(m_{\mathrm{H}})$ is determined as a function of the Higgs boson mass hypothesis: this is the fraction of outcomes of all possible experiments *with signal only* of mass m_{H} for which the

estimator value would be smaller than or equal to that of the experiment under consideration. The expected confidence level for the null hypothesis, $\langle c \rangle_\infty(m_{\rm H})$, is the average value of $c(m_{\rm H})$ for experiments *with background only*. The mass for which $\langle c \rangle_\infty(m_{\rm H})$ crosses the 5% level represents the mass value which, on average, is "excluded at the 95% confidence level" if the true Higgs boson mass is out of reach. The optimization of an analysis is achieved by minimizing $\langle c \rangle_\infty(m_{\rm H})$ with respect to the selection cut values, with $m_{\rm H}$ chosen at the edge of the expected sensitivity domain.

When several analyses are to be combined, the individual optimization of each of them following the method described above does not guarantee that the combination is in turn optimal. In general, this depends on how the combination is performed. The optimal combination method can be defined, as above, as the combination leading to the smallest expected combined confidence level. Therefore, the expected confidence level $\langle c_i \rangle_\infty$ has to be computed for each analysis i as a function of the selection cut values, and the expected combined confidence level simultaneously minimized with respect to the selection cuts of all analyses. The combination procedure is briefly described in the following subsection.

3.3 Analysis Combination

To merge the analyses, the prescription of Ref. [15] is chosen. Let $c_i(m_{\rm H})$, $i = 1, \ldots, n$, be the confidence levels determined on the actual data sample from the n analyses, as a function of the Higgs boson mass hypothesis. If no other information as to the intrinsic capabilities of each of the n analyses is known, it can be shown [15] that the optimal way to combine the n confidence levels is to use the product

$$f(m_{\rm H}) = \prod_{i=1}^{n} c_i(m_{\rm H}).$$

The combined confidence level is obtained by calculating the fraction of outcomes of experiments *with signal only* that would lead to a value of f less than or equal to the measured one.

Although optimal when the qualities of the various analyses are unknown, this democratic approach can lead to an average dilution of the performance of a superior analysis by an inferior one. According to the prescription that the expected combined confidence level has to be minimized, the poor analysis would have to be rejected and ignored in the combination.

To keep such an analysis in the combination, this approach can be refined into an elitist approach by merging the different confidence levels, taking into account the intrinsic capabilities of each of the analyses:

$$f(m_{\rm H}) = \prod_{i=1}^{n} c_i^{a_i}(m_{\rm H}).$$

The optimal "weights" a_i are obtained by minimizing the expected combined confidence level, calculated from the individual expected confidence levels $\langle c_i \rangle_\infty(m_{\rm H})$. These weights guarantee that the confidence level, and hence the mass limit, is never degraded, on average, by the inclusion of additional analyses.

The Higgs boson mass hypothesis $m_{\rm H}^{\rm min}$ that leads to a value of 5% for the measured compound confidence level is the 95% C.L. lower limit on the Higgs boson mass.

4 Event Selection

The selections of the various final states are described in the following subsections. The expected background, efficiency and expected number of signal events for each channel are summarized in Table 2 for a 70 GeV/c^2 Higgs boson. The variation of the efficiency and the expected number of signal events with the Higgs boson mass is shown in Fig. 2. In the $e^+e^- \to Hq\bar{q}$ channel, events in which the Higgs boson decays to tau leptons are explicitly removed, as this final state is selected by the $\tau^+\tau^-q\bar{q}$ analysis.

Table 2: The Higgs-strahlung branching ratio, background, signal efficiency, and the number of signal events expected for a Higgs boson mass of $m_H = 70\,\mathrm{GeV}/c^2$. The left-hand entries are for 161 GeV and the right-hand entries are for 170–172 GeV. The expected number of signal events takes into account the small contributions from WW and ZZ fusion.

Final State	Br.(%)	Background		Efficiency(%)		$\langle n_s \rangle$	
$H\ell^+\ell^-$	6.7	0.06	0.11	64.2	74.8	0.08	0.40
$H\nu\bar{\nu}$	20.0	0.06	0.09	26.3	42.9	0.11	0.70
$Hq\bar{q}$	64.6	0.17	0.23	21.1	21.9	0.24	1.12
$H\tau^+\tau^-$	3.4	0.02	0.02	18.8	20.4	0.01	0.05
$\tau^+\tau^-q\bar{q}$	5.3	0.05	0.03	17.4	17.4	0.02	0.07
Total	100	0.36	0.48	24.7	29.6	0.46	2.34

In the following subsections, the distributions of simulated data are normalized to the collected luminosity and the distributions for the simulated signal are for a Higgs boson mass of 70 GeV/c^2, unless otherwise indicated.

4.1 The $H\ell^+\ell^-$ Final State

The $H\ell^+\ell^-$ final state represents 6.7% of the Higgs-strahlung cross section. Most of the signal events are characterized by two leptons with an invariant mass close to m_Z and a large hadronic recoil mass. The case in which the Higgs boson decays to a tau pair is also considered. Although this channel has a low branching ratio, the experimental signature is clean and the Higgs boson mass can be reconstructed with a good resolution.

4.1.1 Selection

Events are required to have at least four good tracks with $|\cos\theta| < 0.95$ (θ is the polar angle with respect to the beam axis), with a total charged energy larger than $10\%\sqrt{s}$. The selection procedure attempts to reconstruct the Z boson by finding pairs of oppositely charged particles, hereafter referred to as "leptons", which are either identified as electrons or muons [6] or isolated. The isolation angle of a particle is defined as the half-angle of the largest cone around the particle direction containing less than 5% of the total energy of the other particles in the event. In this analysis a particle is isolated if the isolation angle is larger than 10°. To account

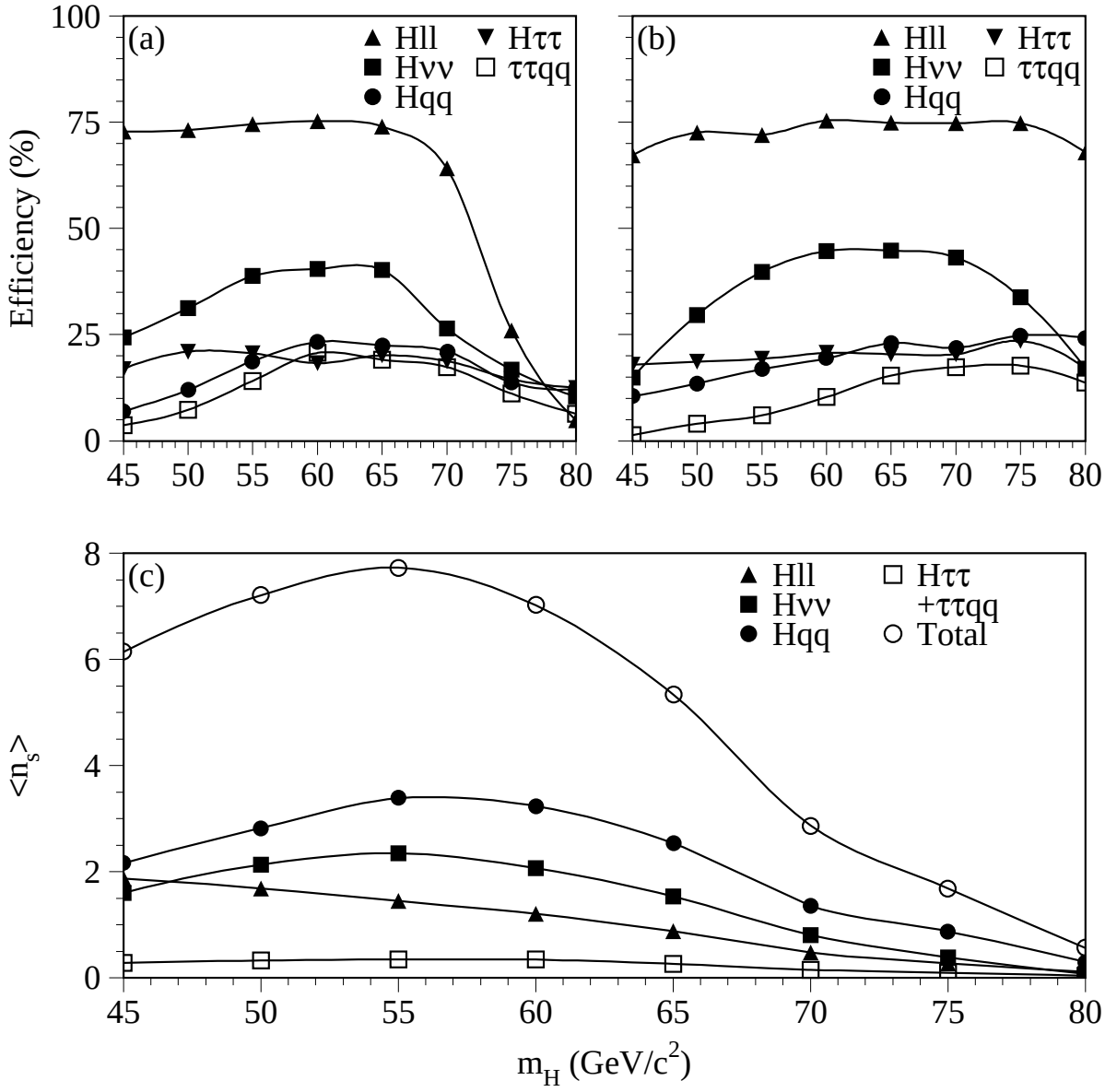

Figure 2: The reconstruction efficiency as a function of the Higgs boson mass at (a) 161 GeV and (b) 172 GeV. (c) The number of expected events for all energies as a function of the Higgs boson mass.

for possible Bremsstrahlung photons, neutral energy-flow particles within 2° of the directions of the lepton momenta are excluded from the isolation calculation. In events with an identified electron, the energy of these neutral particles is added to the electron energy. Combinations with no identified lepton, or with an identified e-μ pair, are rejected.

The Higgs boson mass is calculated as the mass recoiling to the lepton pair. The resolution is improved by including a possible radiative photon from the decay of the Z boson. Such a photon must be isolated and have an energy greater than 2 GeV. The isolation angle is determined in the same way as above, but excluding the leptons from the calculation. If more than one photon is identified, the photon which forms with the leptons the invariant mass closest to m_{Z} is chosen. The reconstructed $\ell^+\ell^-(\gamma)$ mass is required to be greater than 80 GeV/c^2. Figure 3a shows the $\ell^+\ell^-(\gamma)$ invariant mass distribution for the data and the simulation.

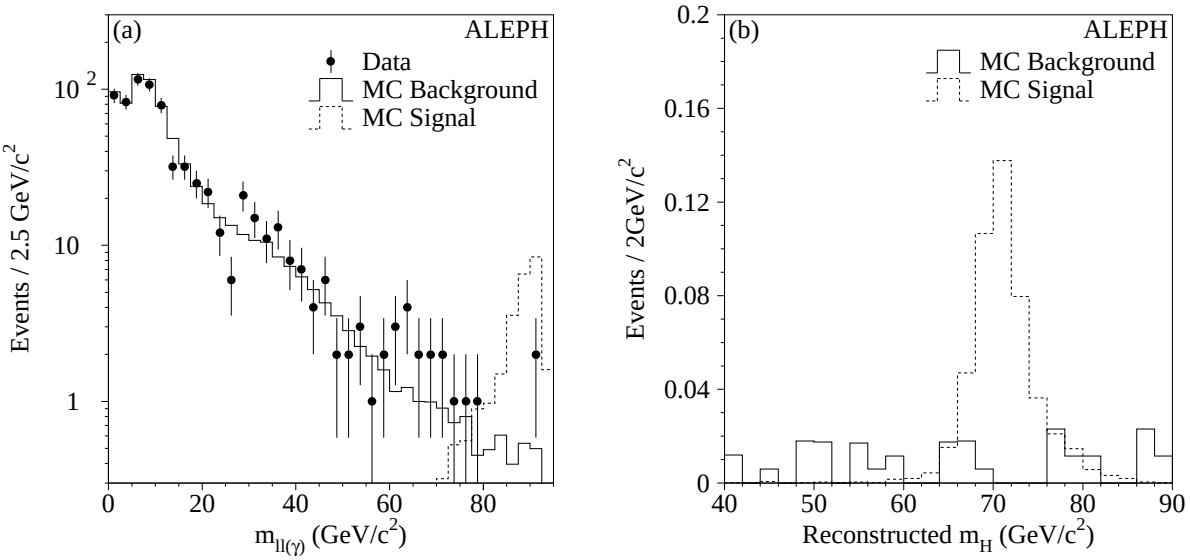

Figure 3: (a) The $\ell^+\ell^-(\gamma)$ mass distribution for the data (points), the background (solid histogram), and the expected signal (dashed histogram), with loosened selection criteria. (b) The distribution of the mass recoiling to the lepton pair after all the selection criteria are applied. The solid histogram is the background and the dashed histogram is the signal.

To reject events with an energetic photon from a radiative return to the Z, the most energetic isolated photon must have an energy less than 40 GeV at $\sqrt{s}$ = 161 GeV, and 45 GeV at $\sqrt{s}$ = 172 GeV. These values correspond to about 75% of the most probable energy of the photon in $\mathrm{e^+e^-} \to \mathrm{q\bar{q}}\gamma$ events.

After selection of the lepton pair, the remaining particles are clustered into two jets using the Durham algorithm. To reject $\mathrm{e^+e^-} \to \mathrm{q\bar{q}}$ events where the leptons are close to the jets, the sum of the transverse momenta of the leptons with respect to their nearest jet is required to be greater than 20 GeV/c.

The visible mass, excluding the particles attributed to the Z decay, must be larger than 15 GeV/c^2. This rejects $\mathrm{e^+e^-}\gamma^*$ and $\mathrm{Z}\gamma^*$ processes with a low γ^* mass. To further reduce this background in events which have only one identified lepton, the track closest in angle to each

lepton candidate must lie within 110°.

Events with exactly four good tracks are candidates for $(H \to \tau^+\tau^-)\ell^+\ell^-$ and are required to have a missing energy of at least $7\%\sqrt{s}$.

In events with only one identified lepton, both leptons are required to be isolated and their invariant mass should be greater than $85\,\mathrm{GeV}/c^2$. Furthermore, the background from $WW \to q\bar{q}\ell\nu$ events is rejected by explicitly reconstructing the W's. The missing four-momentum (neutrino) and the lepton are assigned to the leptonic W, and the remaining energy flow particles to the hadronic W. Events where the mass sum of the reconstructed W's is greater than $150\,\mathrm{GeV}/c^2$ and where the mass of the hadronic W is less than $90\,\mathrm{GeV}/c^2$ are rejected.

The background expected with a mass recoiling against the lepton pair larger than $50\,\mathrm{GeV}/c^2$ is 0.06 and 0.11 events at 161 GeV and 170–172 GeV, respectively. Figure 3b shows the Higgs boson mass distribution for the simulation. No events are observed in the data.

4.1.2 Systematic Uncertainties

Potential sources of systematic uncertainties include lepton identification, lepton isolation, and energy and momentum reconstruction. The lepton identification efficiency has been studied and the effect on the selection efficiency is less than 0.2%. The lepton isolation criterion is tested by studying hadronic events with identified leptons. Good agreement is observed between the data and simulation and no uncertainty is assigned. The energy resolution of photons and electrons in the electromagnetic calorimeter and the momentum resolution for muons are studied using $e^+e^- \to \ell^+\ell^-$ events and are found to be slightly better in the simulation. Corrections are applied and the uncertainty on the efficiency is estimated to be less than 0.3%. Taking the aforementioned uncertainties as independent, the total relative systematic uncertainty on the selection efficiency is 0.4%.

4.2 The $H\nu\bar{\nu}$ Final State

The $H\nu\bar{\nu}$ final state comprises 20.0% of the total Higgs-strahlung cross section. These events are characterized by large missing mass compatible with the Z mass, and two acoplanar jets.

4.2.1 Selection

The event selection requires hadronic events with a missing mass larger than $80\,\mathrm{GeV}/c^2$, and a visible mass less than $75\,\mathrm{GeV}/c^2$. Background from two-photon collisions is reduced by requiring the visible mass to be larger than $30\%\sqrt{s}$ or the total transverse momentum to be larger than $5\%\sqrt{s}$.

Events with undetected energetic particles at low polar angles are rejected by requiring the angle between the missing momentum and the beam axis to be larger than 25°. Also, the longitudinal missing momentum must be less than $20\,\mathrm{GeV}/c$ and $30\,\mathrm{GeV}/c$, respectively, at 161 GeV and 170–172 GeV.

Background from radiative returns to the Z is further reduced by means of the event acoplanarity. Events are first divided into hemispheres using the plane perpendicular to the thrust axis and non-zero energy is required in each of the hemispheres. The event acoplanarity is defined as the absolute value of the triple product of the normalized momentum vector of each hemisphere and the unit vector along the beam axis. This can be expressed as $|\sin\theta_1 \sin\theta_2 \sin(\phi_1 - \phi_2)|$, where $\theta_{1,2}$ and $\phi_{1,2}$ are respectively the polar and azimuthal angles of the momentum vectors. The acoplanarity is required to be larger than 0.12. Figure 4a shows the distribution of the acoplanarity for the data and the simulation.

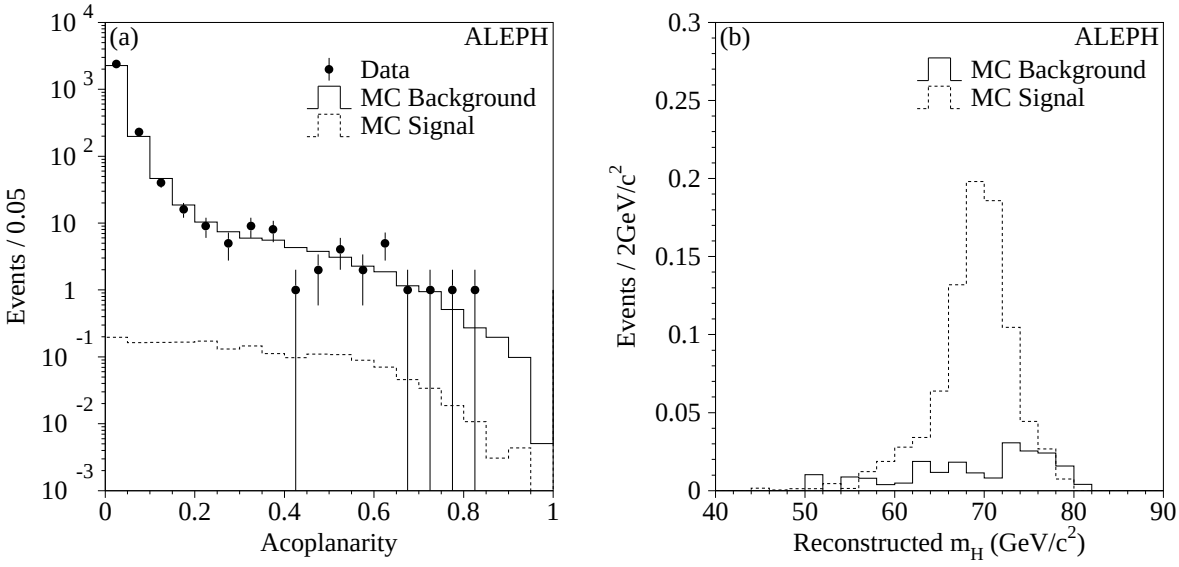

Figure 4: (a) The event acoplanarity distribution for the data (points), background (solid histogram), and signal (dashed histogram). (b) The distribution of the reconstructed Higgs boson mass for background (solid histogram), and signal (dashed histogram). All selection criteria are applied except the requirement on the visible mass.

Events from processes such as Weν, Zee and two-photon collisions where energetic electrons are scattered into the detector are removed by the requirement that the observed energy within 12° of the beam axis be less than $3\%\sqrt{s}$.

To remove background from hadronic events with energetic neutrinos from semileptonic decays of b or c hadrons, the energy contained in an azimuthal wedge of half angle 30° with respect to the plane defined by the beam and the missing momentum direction must be less than $10\%\sqrt{s}$.

The remaining background is reduced using b tagging. The b tagging algorithm described in Ref. [10] is slightly modified, however, to avoid associating a hadron jet from one W in $\mathrm{WW} \to \mathrm{qq}\ell\nu$ events with the lepton from the other W, and possibly tagging the hadron jet as a b quark jet. Leptons with $p_t > 1.5\,\mathrm{GeV}/c$ with respect to the associated jet are not considered for the purposes of b tagging. The sum of the neural network outputs for the two hemisphere jets is required to satisfy $\eta_1 + \eta_2 > 1.1$.

To further reduce background from $\mathrm{WW} \to \mathrm{qq}\tau\nu$ events, jets are reconstructed using the

JADE clustering algorithm with a $y_{\rm cut}$ of m_τ^2/s. The most isolated jet is required to have an energy less than 5 GeV.

The expected background is 0.06 and 0.09 events at 161 GeV and 170–172 GeV, respectively. Figure 4b shows the reconstructed Higgs boson mass distribution for the simulation. No events are observed in the data.

4.2.2 Systematic Uncertainties

The requirement on the maximum observed energy within 12° of the beam axis was studied in random trigger events and is found to reduce the signal efficiency by 0.5%.

The effect of the underlying physics distributions on the b tagging is studied by varying the momenta and lifetimes of the b hadrons in the simulation within their uncertainties. The b hadron momentum spectrum in the simulation is varied within the uncertainties quoted in Ref. [16] and the effect on the selection efficiency is 0.4%. The lifetimes of the weakly-decaying b hadrons are varied about the world-average lifetime of 1.55 ± 0.02 ps [17], and the effect is found to be negligible. The uncertainty on the b tagging efficiency due to the simulation of the detector response is investigated by studying the track impact parameter resolution, since it provides the bulk of the b tagging information. An additional smearing of the track parameters, described in Ref. [10], is introduced in the simulation to correct for discrepancies in the impact parameter resolution. This decreases the efficiency in the simulation by 0.4%, and a systematic uncertainty corresponding to half of this variation is assigned.

Uncertainties coming from the simulation of non-b tagging variables have been extensively studied [2]. The overall uncertainty was found to be less than 1%.

Taking these uncertainties as independent, the total relative systematic uncertainty on the selection efficiency is 1.1%.

4.3 The $\mathrm{Hq\bar{q}}$ Final State

The $\mathrm{Hq\bar{q}}$ final state accounts for 64.6% of the Higgs-strahlung cross section, not including the case where the Higgs boson decays to tau leptons. The events are characterized by two jets from the Z decay accompanied by two jets from the Higgs boson decay. The main sources of background are $\mathrm{e^+e^-} \to \mathrm{q\bar{q}}(\gamma)$, $\mathrm{e^+e^-} \to \mathrm{W^+W^-}$ and $\mathrm{e^+e^-} \to \mathrm{ZZ}$.

4.3.1 Selection

The standard hadronic event selection criteria are tightened to at least eight good tracks satisfying $|\cos\theta| < 0.95$. The events are forced to form four jets by the Durham jet-clustering algorithm and the $y_{\rm cut}$ value where the transition from four to three jets occurs (y_{34}) must be larger than 0.004.

Radiative returns to the Z with energetic undetected photons at low polar angles are removed by requiring the missing momentum along the beam direction to be smaller than $1.5\,(m_{\rm vis} - 90)$,

where $m_{\rm vis}$ is the invariant mass in GeV/c^2 of all the energy-flow particles. Radiative returns to the Z where energetic photons are observed in the detector are removed by identifying the electromagnetic clusters due to these photons. The electromagnetic energy is computed from identified photons and electrons, charged particle pairs consistent with photon conversions, neutral particles passing through an electromagnetic calorimeter crack region and detected in the hadron calorimeter, and particles detected in the luminosity monitors. If the fraction of electromagnetic energy in a one degree cone around any energy flow particle in a given jet is larger than 80% of the jet energy, the event is rejected. Each jet is further required to contain at least one good track.

In order to reject background events in which three of the jets are close in angle, as expected in $\mathrm{e^+e^-} \to \mathrm{q\bar{q}}$ events, the sum Θ of the four smallest jet-jet angles must be larger than 350°.

Near threshold the Higgs and Z bosons decay into a pair of approximately back-to-back jets. The sum of the cosines of the opening angles of the two jet pairs, therefore, discriminates between a signal close to threshold and the background from Z decays to hadrons. Since the correct pairing is not known *a priori*, the minimum value over all possible jet-jet combinations is used: $\gamma = \min\left(\cos\theta_{ij} + \cos\theta_{kl}\right)$ for all permutations of $ijkl$. Events are required to satisfy $\gamma < -1.2$ at 161 GeV and $\gamma < -0.9$ at 170–172 GeV.

The energies of the four jets are rescaled by imposing energy-momentum conservation, fixing the four jet velocities to their measured values. If any of the rescaled energies is negative because the measured jet directions are not compatible with a four-body final state, the observed momentum and energy of all four jets are used instead.

At 161 GeV, at least one of the six possible jet pairing combinations is required to satisfy either of the following sets of criteria, referred to as a) and b):

a)
- $y_{34} > 0.008$
- $m_{12} > 82\,\mathrm{GeV}/c^2$ (Z boson candidate)
- $m_{34} > 45\,\mathrm{GeV}/c^2$ (Higgs boson candidate)
- $\min\left(\eta_3, \eta_4\right) > 0.6$
- $(1-\eta_3)(1-\eta_4) < 8 \times 10^{-3}$

b) $1.9\,y_{34} + 0.14 \sum_{i=1}^{4} \eta_i > 0.48.$

The variables m_{12} and m_{34} are respectively the invariant masses of jet pairs corresponding to the Z and Higgs boson candidates and $\{\eta_i\}$ are the b tagging neural network outputs [10]. The requirement b) is similar to that used in Ref. [10] and is designed to select four b quark final states.

At 170–172 GeV, the requirements on the Z boson mass and the b tagging are modified to take into account the different level and composition of the background:

a′)
- $y_{34} > 0.008$
- $m_{12} > 80\,\mathrm{GeV}/c^2$

- $m_{34} > 45\,\mathrm{GeV}/c^2$
- $\min(\eta_3, \eta_4) > 0.6$
- $(1-\eta_3)(1-\eta_4) < 4 \times 10^{-3}$

b′) $1.9\, y_{34} + 0.14 \sum_{i=1}^{4} \eta_i > 0.52.$

Figure 5a shows the distribution of the b tagging variable $(1-\eta_3)(1-\eta_4)$. The expected background is 0.17 and 0.23 events at 161 GeV and 170–172 GeV, respectively. Figure 5b shows the reconstructed Higgs boson mass distribution. No events are observed in the data.

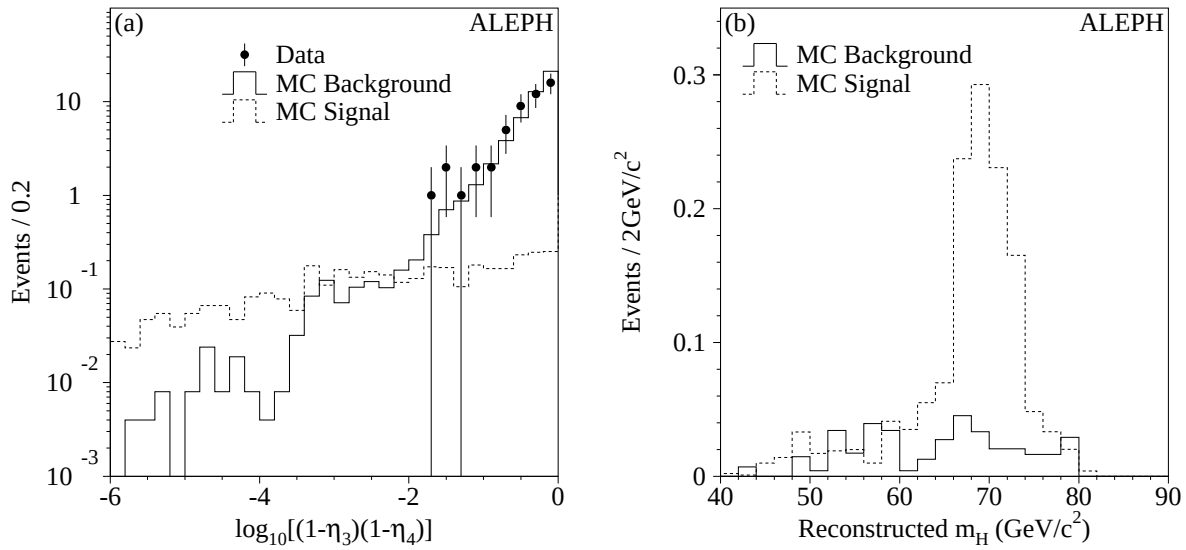

Figure 5: (a) The distribution of the b tagging variable $(1-\eta_3)(1-\eta_4)$ at 170–172 GeV, for the data (points), the simulated background (solid histogram), and the signal (dashed histogram). All cuts are applied except the b tagging criteria in a′). If more than one combination in an event is selected, the combination with the smallest value of $(1-\eta_3)(1-\eta_4)$ is plotted. (b) The distribution of the reconstructed Higgs boson mass $m_{12} + m_{34} - 91.2\,\mathrm{GeV}/c^2$ for the background (solid histogram) and the signal (dashed histogram), summed over the centre-of-mass energies. The plot shows only the combination for which m_{12} is closest to the nominal Z mass.

An alternative event selection based on a neural network has also been developed. Its performance is similar to the standard analysis described above, though it is not used to derive the final result presented in this letter because it leads to a minimum value of $\langle c \rangle_\infty$ slightly larger than the standard selection.

In the neural network analysis, the selection of hadronic events, the determination of the jet four-momenta, and the rejection of background from radiative returns to the Z are adopted from the standard selection. Only events satisfying $y_{34} > 0.008$ are considered.

The neural network inputs include the following variables, used in the standard analysis: $\{\eta_i\}$, y_{34}, Θ, and γ. The reconstructed Higgs boson mass variable m_{34} is not used, to avoid

biasing of the neural network selection toward a given m_{H} value. Additional inputs to the neural network include the probability that the impact parameters of the tracks in the event are consistent with zero lifetime [8], the event thrust and sphericity, the track multiplicity, the minimum dijet mass, and the minimum values of the following jet properties: mass, energy and track multiplicity.

These variables discriminate between signal and background without assigning the jets to the Higgs or Z boson candidates. This information is used together with the mass m_{12} of the Z boson candidate and the b tagging information for each of the six possible jet pairings. The neural network discriminates signal from background and selects the most probable H and Z candidates among the six combinations in each event. Events are selected by placing a cut on the output of the neural network.

The expected background is 0.12 and 0.32 events at 161 GeV and 170–172 GeV, respectively. The background as a function of the reconstruction efficiency is shown for the standard analysis and the neural network analysis in Fig. 6. This selection also does not select any events in the data.

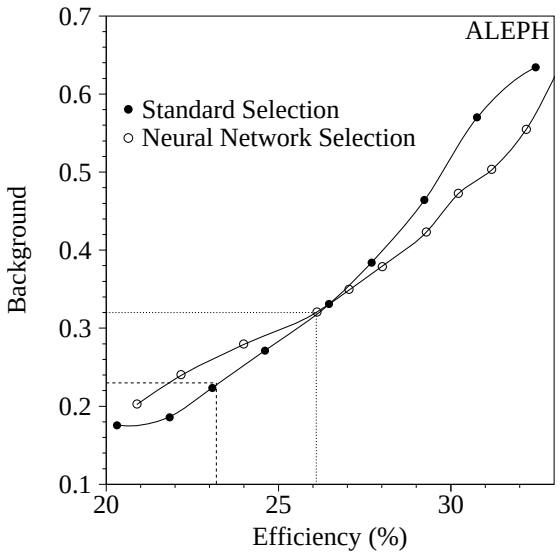

Figure 6: The expected background as a function of the efficiency for the two four-jet analyses for a Higgs boson of mass 67 GeV/c^2 and a centre-of-mass energy of 172 GeV. The dashed and dotted lines indicate the working points of the standard and the neural network analyses, respectively. The curve for the standard analysis (solid points) is obtained by varying the cuts on m_{12} and the b tagging variables. The curve for the neural network analysis (hollow points) is obtained by varying the cut on the neural network output.

4.3.2 Systematic Uncertainties

The determination of the systematic uncertainty arising from the b tagging follows the prescription of Section 4.2.2. The variation of the b hadron momentum spectrum in the

simulation results in a 1.0% uncertainty. The lifetime uncertainty is negligible, as was the case previously. The uncertainty due to impact parameter resolution is 0.8%.

The modelling of the non-b tagging variables is studied using the sample of events obtained after the selection of hadronic events and the rejection of radiative returns to the Z. The signal distributions are reweighted using weights calculated from a comparison of the data and the background simulation. No statistically significant deviations are found and a systematic uncertainty of 1.2% is attributed to this source.

Adding the above uncertainties in quadrature results in an overall relative systematic uncertainty on the selection efficiency of 1.8%.

4.4 The H$\tau^+\tau^-$ and $\tau^+\tau^-$q$\bar{\text{q}}$ Final States

The H$\tau^+\tau^-$ final state accounts for 3.4% of signal decays, including final states with four tau leptons. The $\tau^+\tau^-$q$\bar{\text{q}}$ channel has a branching ratio of 5.3%, including the hadronic branching ratio of the Z. Non-hadronic decays of the Z are not considered here as they are addressed by other channels described in this letter.

The selection procedure begins with a common set of criteria sensitive to $\tau^+\tau^-$q$\bar{\text{q}}$ final states produced via either process. This preselection is similar to the track based selection developed for hA $\rightarrow \tau^+\tau^-$q$\bar{\text{q}}$ [10], but with looser criteria. Further criteria are then applied, tailored to the channel under consideration.

4.4.1 Preselection

Hadronic events are selected by requiring at least five good tracks with $|\cos\theta| < 0.95$ which account for at least 10% of $\sqrt{s}$. Radiative returns with undetected photons at low polar angles are rejected by requiring the longitudinal missing momentum to be less than $40\,\text{GeV}/c$. The signal events are also characterized by missing energy due to the undetected neutrinos. This is exploited by requiring the measured missing energy to be positive.

The identification and reconstruction of tau lepton candidates is identical to that of Ref. [10]. Events are required to have at least two tau candidates of opposite charge, and at least one of the tau jets is required to have unit charged multiplicity. The sum of the isolation angles of the tau candidates is required to be larger than 50°. The isolation angle is defined as the half-angle of the largest cone about the tau candidate direction containing less than 5% of the total energy of the particles in the event excluding the particles (neutral and charged) making up the tau.

In events with one identified lepton, background from WW $\rightarrow$ qq$\ell\nu$ events is rejected using the method described in Section 4.1. The cuts on the mass sum and the hadronic mass are set to $140\,\text{GeV}/c^2$ and $85\,\text{GeV}/c^2$, respectively.

Energy-flow particles not included in the tau jets are clustered into two jets with the Durham algorithm. A χ^2 fit is performed on the event using a modified version of the method described in Ref. [10]. Here, a constraint on the compatibility of the $\tau^+\tau^-$ or q$\bar{\text{q}}$ pair masses with the

nominal Z mass is imposed, depending on the channel under consideration. If more than one combination passes the selection criteria, the combination with the smallest χ^2 is kept. The fitted mass of the pair assigned to the Higgs boson decay is required to lie between $40\,\mathrm{GeV}/c^2$ and $80\,\mathrm{GeV}/c^2$. Figure 7a shows the distribution of the χ^2 variable for the data and the simulation after the preselection.

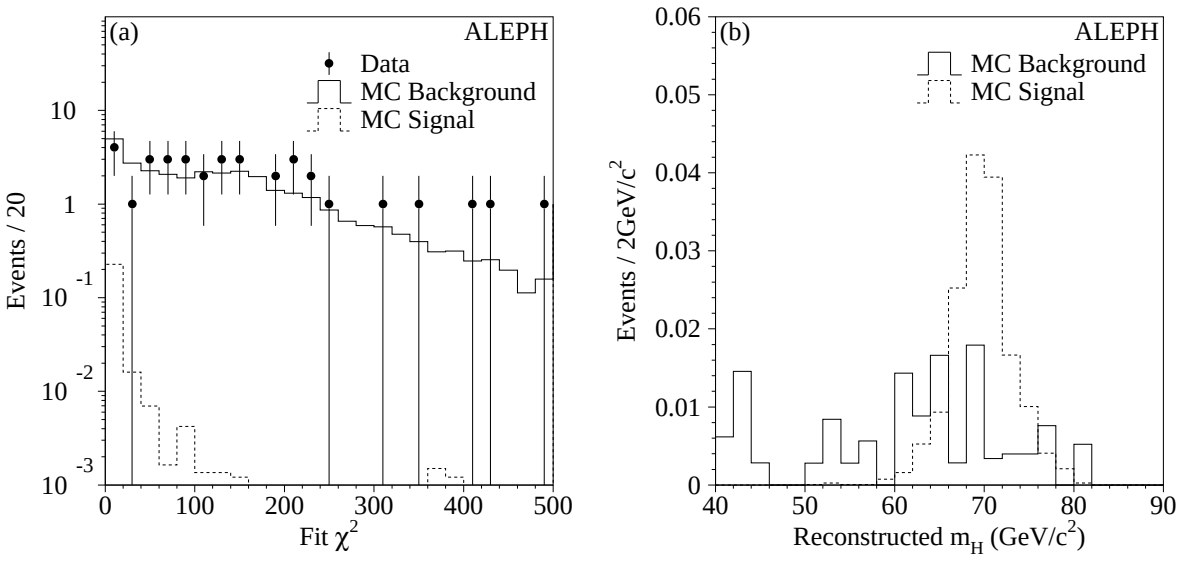

Figure 7: (a) The fit χ^2 variable for the $\mathrm{H} \to \tau^+\tau^-, \mathrm{Z} \to \mathrm{q\bar{q}}$ channel after the preselection. The points are the data, the solid histogram is the expected background, and the dashed histogram is the signal. (b) The distribution of the fitted Higgs boson mass for both channels after the selection criteria have been applied. The solid histogram is the expected background and the dotted histogram is the signal. The cuts on the reconstructed Higgs boson mass are relaxed.

4.4.2 $\mathbf{H\tau^+\tau^-}$

Two further criteria are applied to select signal decays in this channel. The χ^2 of the fit is required to be less than 20 and the neural network b tag values for the non-tau jets are required to satisfy $\eta_1 + \eta_2 > 1$.

The expected background for the collected luminosity is 0.02 and 0.02 events at 161 GeV and 170–172 GeV, respectively. No events are selected in the data.

4.4.3 $\boldsymbol{\tau^+\tau^-\mathrm{q\bar{q}}}$

The inapplicability of b tagging in this channel leads to a tightening of the preselection requirements and a larger set of additional selection criteria.

To reduce background from low multiplicity hadron jets misidentified as tau jets, no good tracks are allowed to fall within a 30° cone around the tau candidate direction. Furthermore, the sum of the masses of the tau candidates must not exceed $1.5\,\mathrm{GeV}/c^2$.

The χ^2 of the fit is required to be less than 10 and the fitted energies of the non-tau jets must be larger than 85% of the measured values. The angle between the two tau candidates is required to be larger than 120°. To reduce the background from the process $e^+e^- \to e^+e^-Z$ where typically one high momentum electron is unobserved due to its low polar angle, the missing energy is required to be less than 75 GeV .

The expected background for the collected luminosity is 0.05 and 0.03 events at 161 GeV and 170–172 GeV, respectively. No events are observed in the data.

Figure 7b shows the reconstructed Higgs boson mass distribution for the simulation. The results of the selections of both channels contributing to this final state have been added.

4.4.4 Systematic Uncertainties

The main sources of systematic uncertainty are energy flow reconstruction and b tagging. Inaccuracies of the simulation of the reconstructed energy flow particles can cause systematic differences in the simulated efficiency. In particular, they might affect the efficiency of a cut on the reconstructed Higgs boson mass and also the requirements on the value of the fit χ^2. This is studied by introducing additional smearing to the measured momenta of the reconstructed tau and non-tau jets and redoing the fit. The effect is found to be negligible even when the additional smearing is much larger than the effect of any possible inaccuracies of the simulation.

The simulation of the b tagging affects only the $H\tau^+\tau^-$ channel. The determination of the systematic uncertainty has already been described in Section 4.2.2 and results in a 3.0% relative error on the efficiency.

Therefore, a relative uncertainty of 3.0% for the $H\tau^+\tau^-$ channel results, with no significant uncertainty for the $\tau^+\tau^-q\bar{q}$ channel.

5 Combined Results

No candidate events are retained in any of the selections presented in the previous section, in agreement with the 0.84 events expected from Standard Model processes. In the absence of any signal, the results of the five selections are combined as outlined in Section 3.3 to set a 95% C.L. lower limit on the Higgs boson mass.

The measured and expected confidence levels are computed at both centre-of-mass energies (161 and 170–172 GeV) for each of the five analyses. Since no candidate events are selected by any analysis, the measured confidence levels are simply $\exp(-s_i)$, where s_i is the number of signal events expected to be selected by the i-th analysis. The two centre-of-mass energies are first combined for each of the final states, and then the five analyses together. In these two successive combinations, the democratic ($a_i = 1$) and the elitist (optimal a_i's) approaches give essentially identical results. This is due to the analysis optimization procedure that optimizes the expected combined confidence level rather than the individual ones, as already described in Sec. 3.2. The result is displayed in Fig. 8a. While no single analysis allows a confidence level smaller than 5% to be reached in a significant mass domain, the combination excludes the

whole range between 45 and 69.4 GeV/c^2 at more than 95% C.L.

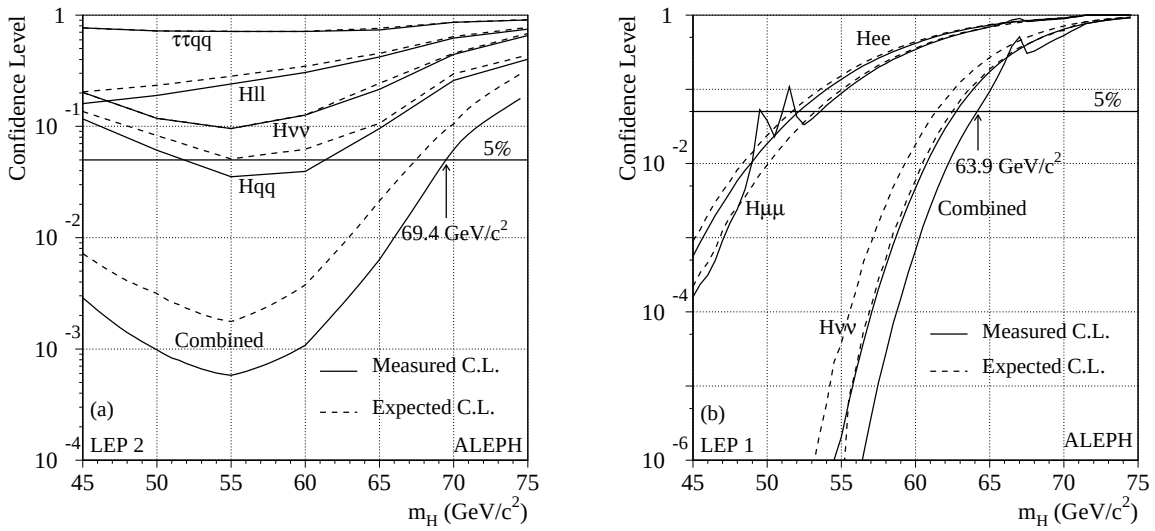

Figure 8: The measured (full curves) and expected (dashed curves) confidence levels for each of the final states, and their combination, (a) at high energy and (b) at LEP 1. The H$\tau^+\tau^-$ and $\tau^+\tau^-$q$\bar{\text{q}}$ analyses are combined into a single $\tau^+\tau^-$q$\bar{\text{q}}$ result.

The same procedure is then applied to the three selections (for the He$^+$e$^-$, H$\mu^+\mu^-$ and H$\nu\bar{\nu}$ final states) developed for the LEP 1 data analysis [2]. Here, three candidate events were observed in the H$\mu^+\mu^-$ channel. They can be seen as bumps in the measured confidence levels displayed in Fig. 8b. The weight assigned to the H$\nu\bar{\nu}$ final state turns out to be about five times smaller than the weights assigned to the H$\ell^+\ell^-$ final states, mainly due to the superior mass resolution achieved in the leptonic channels. A 95% C.L. lower limit on the Higgs boson mass of 63.9 GeV/c^2 is found, the same as in Ref. [2].

Finally, the LEP 1 and LEP 2 results are combined. The weight assigned to the high energy part is found to be at least 20% larger than that assigned to LEP 1, slowly increasing with the Higgs boson mass hypothesis and becoming very large above 71 GeV/c^2, where the H$\ell^+\ell^-$ LEP 1 selection has no efficiency. The resulting confidence levels (measured and expected) are shown in Fig. 9. Higgs boson masses below 70.7 GeV/c^2 are excluded at more than 95% C.L.

This result can also be viewed in Fig. 10, where the number of signal events expected is displayed as a function of the Higgs boson mass, together with N_{95}, the number of signal events needed to exclude the corresponding mass hypothesis at 95% C.L.

The sources of systematic uncertainties on the number of signal events expected are

- An uncertainty of $\pm 0.5\%$ from the total integrated luminosity measurement.
- The centre-of-mass energy is affected by an uncertainty of ± 0.054 GeV [18], which corresponds to a $\pm 0.3\%$ variation in the signal cross section.

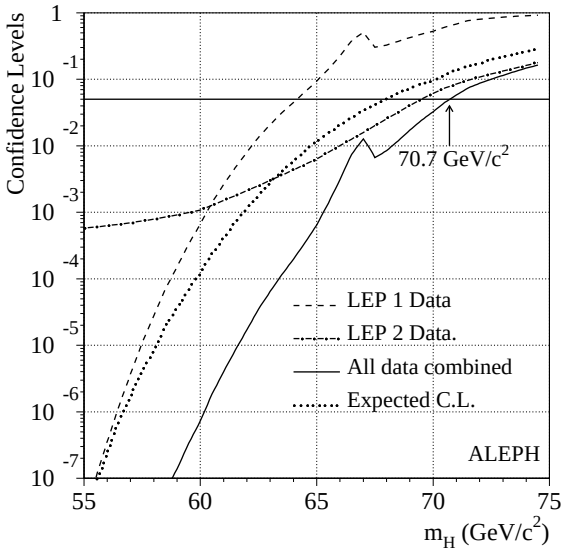

Figure 9: Measured confidence level curves for the high energy data (dash-dotted), the LEP 1 data (dashed), and the combination (full). The dotted curve shows the expectation for the combination.

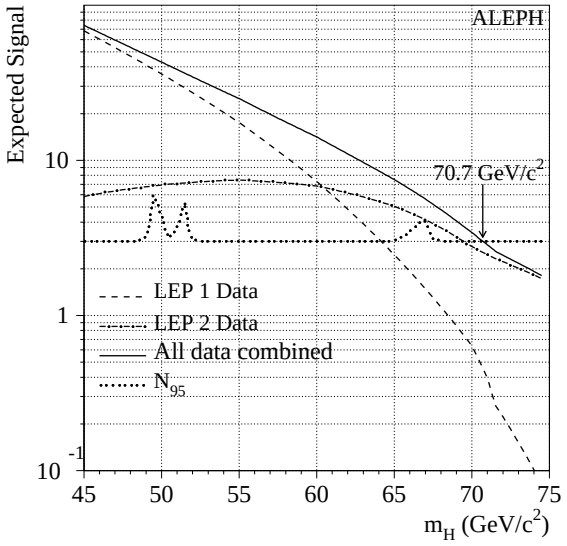

Figure 10: Number of events expected for signal from high energy data (dash-dotted curve), LEP 1 data (dashed curve), and the combination (full curve). The dotted curve indicates the number of signal events needed to reach a confidence level of 5%. The bumps are due to the three candidate events found at LEP 1 in the $H\mu^+\mu^-$ channel.

- The knowledge of the top quark mass, $m_{\rm top} = 175 \pm 6$ GeV/c^2 [19], the simulation of the initial state radiation, and the comparisons between different Monte Carlo programs [20] result in an uncertainty of $\pm 1\%$ in the signal cross section.
- The ambiguities on the values of the b and c quark masses entering the calculation of the $(\mathrm{H} \to \mathrm{b\bar{b}})$ and $(\mathrm{H} \to \mathrm{c\bar{c}})$ decay partial widths introduce a $\pm 1\%$ uncertainty on the corresponding branching ratios. This translates into $\pm 0.7\%$ for the number of signal events expected.
- The limited signal Monte Carlo statistics induce an uncertainty of 0.5%.
- The uncertainty related to the selection procedures, detailed in the previous sections, is smaller than 2%.

The overall systematic uncertainty is therefore below $\pm 3\%$. Following the method of Ref. [21], this results in a small increase of the measured confidence level, corresponding to a change of the mass limit by about 10 MeV/c^2.

6 Conclusion

The reaction $\mathrm{e^+e^-} \to \mathrm{HZ}$ was used to search for the Standard Model Higgs boson. The data sample consists of integrated luminosities of 10.9 pb^{-1}, 1.1 pb^{-1} and 9.5 pb^{-1}, collected at centre-of-mass energies of 161 GeV, 170 GeV and 172 GeV, respectively. No candidate events were found in any of the final states, in agreement with the 0.84 events expected from all Standard Model processes. The 95% C.L. lower limit on the Higgs boson mass is 69.4 GeV/c^2. When combined with earlier ALEPH searches performed at LEP 1, the limit increases to 70.7 GeV/c^2.

Acknowledgements

We wish to thank our colleagues from the accelerator divisions for the successful high energy operation of LEP. We are indebted to the engineers and technicians in all our institutions for their contribution to the excellent performance of ALEPH. Those of us from non-member countries thank CERN for its hospitality.

References

[1] See for instance:
J.F. Gunion, H.E. Haber, G. Kane, and S. Dawson, *"The Higgs Hunter's Guide"*, Addison-Wesley (1990);
P.J. Franzini et al., in *"Z Physics at LEP 1"*, eds G. Altarelli, R. Kleiss and C. Verzegnassi, CERN 89-08 (1989);
E. Gross, B.A. Kniehl and G. Wolf, *Z. Phys.* **C63** (1994) 417, and *erratum* **C66** (1995) 32.

[2] ALEPH Collaboration, *Phys. Lett.* **B384** (1996) 427.

[3] OPAL Collaboration, *Z. Phys.* **C73** (1997) 189;
L3 Collaboration, *Phys. Lett.* **B385** (1996) 454;
DELPHI Collaboration, *Nucl. Phys.* **B421** (1994) 3.

[4] OPAL Collaboration, *Phys. Lett.* **B393** (1997) 231.

[5] ALEPH Collaboration, *Nucl. Instrum. Methods* **A294** (1990) 121.

[6] ALEPH Collaboration, *Nucl. Instrum. Methods* **A360** (1995) 481.

[7] D. Creanza et al., *"Construction and Performance of the New ALEPH Vertex Detector"*, to appear in the Proceedings of the Conference on Advanced Technology and Particle Physics, Como, Italy, October 7-11, 1996.

[8] ALEPH Collaboration, *Phys. Lett.* **B313** (1993) 535.

[9] ALEPH Collaboration, *Nucl. Instrum. Methods* **A346** (1994) 461.

[10] ALEPH Collaboration, *"Search for the Neutral Higgs Bosons of the MSSM in* e^+e^- *Collisions at* $\sqrt{s}$ *from 130 to* 172 GeV*"*, CERN PPE 97-XXX, submitted to *Physics Letters* **B**.

[11] This generator is based on the differential cross-section published in:
S. Ambrosanio and B. Mele, *Nucl. Phys.* **B374** (1992) 3.

[12] T. Sjöstrand, *The PYTHIA 5.7 and JETSET 7.4 Manual*, LU-TP.95/20, CERN-TH.7112/93; and *Comput. Phys. Commun.* **82** (1994) 74.

[13] P. Janot, *"The HZHA generator"*, in *"Physics at LEP2"*, Eds. G. Altarelli, T. Sjöstrand and F. Zwirner, CERN 96-01 (1996), Vol. 2, p. 309.

[14] J.-F. Grivaz and F. Le Diberder, *Nucl. Instrum. Methods* **A333** (1993) 320.

[15] P. Janot and F. Le Diberder, *"Combining 'Limits' "*, CERN PPE 97-053 and LPNHE 97-01, to be submitted to *Nucl. Instrum. Methods.*

[16] ALEPH Collaboration, *Phys. Lett.* **B357** (1995) 699.

[17] Particle Data Group, R.M. Barnett et al., *Phys. Rev.* **D 54** (1996).

[18] Working group on LEP energy, private communication.

[19] J. Lys (for CDF Coll.), S. Protopopescu (for D0 Coll.) and P. Tipton, talks given at ICHEP96, Warsaw, 25-31 July 1996, to appear in the proceedings.

[20] M. Carena, P.M. Zerwas et al., *"Higgs Physics"*, in Physics at LEP 2, eds. G. Altarelli, T. Sjöstrand and F. Zwirner, CERN 96-01 (1996) 351.

[21] R.D. Cousins and V.L. Highland, *Nucl. Instrum. Methods* **A320** (1992) 331.